



# Ultrafast transient absorption and solvation of a super-photoacid in acetoneous environments

Johannes Knorr<sup>4,5</sup> · Niklas Sülzner<sup>2,4</sup> · Bastian Geissler<sup>1,4</sup> · Christian Spies<sup>3,4</sup> · Alexander Grandjean<sup>3</sup> · Roger Jan Kutta<sup>1</sup> · Gregor Jung<sup>3</sup> · Patrick Nuernberger<sup>1,4</sup>

Received: 11 May 2022 / Accepted: 8 August 2022 / Published online: 30 September 2022  
© The Author(s) 2022

## Abstract

The phenomenon of photoacidity, i.e., an increase in acidity by several orders of magnitude upon electronic excitation, is frequently encountered in aromatic alcohols capable of transferring a proton to a suitable acceptor. A promising new class of neutral super-photoacids based on pyranine derivatives has been shown to exhibit pronounced solvatochromic effects. To disclose the underlying mechanisms contributing to excited-state proton transfer (ESPT) and the temporal characteristics of solvation and ESPT, we scrutinize the associated ultrafast dynamics of the strongest photoacid of this class, namely tris(1,1,1,3,3,3-hexafluoropropan-2-yl)8-hydroxypyrene-1,3,6-trisulfonate, in acetoneous environment, thereby finding experimental evidence for ESPT even under these adverse conditions for proton transfer. Juxtaposing results from time-correlated single-photon counting and femtosecond transient absorption measurements combined with a complete decomposition of all signal components, i.e., absorption of ground and excited states as well as stimulated emission, we disclose dynamics of solvation, rotational diffusion, and radiative relaxation processes in acetone and identify the relevant steps of ESPT along with the associated time scales.

## Graphical abstract



## 1 Introduction

Upon electronic excitation, so-called photoacids show a higher acidity, i.e., a higher tendency to release an acidic proton, caused by changes in the molecule's electronic

This article is dedicated to Prof. Dr. Silvia E. Braslavsky, a pioneer in photobiology and photobiophysics, on the occasion of her 80th birthday.

✉ Patrick Nuernberger  
patrick.nuernberger@ur.de

<sup>1</sup> Institut für Physikalische und Theoretische Chemie, Universität Regensburg, Universitätsstraße 31, 95053 Regensburg, Germany

<sup>2</sup> Lehrstuhl für Theoretische Chemie, Ruhr-Universität Bochum, 44780 Bochum, Germany

<sup>3</sup> Biophysikalische Chemie, Universität des Saarlandes, 66123 Saarbrücken, Germany

<sup>4</sup> Physikalische Chemie II, Ruhr-Universität Bochum, 44780 Bochum, Germany

<sup>5</sup> Erlangen Graduate School in Advanced Optical Technologies (SAOT), Friedrich-Alexander-Universität Erlangen-Nürnberg (FAU), Paul-Gordan-Straße 6, 91052 Erlangen, Germany

distribution that in turn affect corresponding hydrogen bonds. In 1965, Trieff and Sundheim introduced the term excited-state proton transfer (ESPT) [1]. However, more than 30 years earlier, it was Weber who observed that changing the pH value in a solution containing 1,4-naphthylaminosulfonate leads to changes in the corresponding fluorescence spectrum, while leaving the absorption spectrum unaltered [2]. A few years later, Förster was able to assign this phenomenon to a difference in the protolytic equilibria in the molecular electronic ground and excited state, respectively. Consequently, he introduced the so-called Förster cycle which explains the basic processes occurring in photoacid systems [3, 4]. For these molecules, which are typically weak acids in their ROH form, electronic excitation decreases the  $pK_a$  value by several orders of magnitude. The Förster cycle illustrates the existence of two different species in the excited state, namely the ROH\* and the RO<sup>-\*</sup> species, whereby the asterisk denotes the excited state. Their different energetic positions give rise to two separate emission bands for relaxation back to the respective ground states. Given that the  $pK_a$  value is known, the Förster cycle directly reveals the  $pK_a^*$  value of the photoacid system. If the  $pK_a$  value is unknown, however, still the change in acidity upon photoexcitation can be evaluated [5].

ESPT is always linked to the presence of a suitable acceptor such as a polar solvent molecule. Most studies on ESPT were conducted in aqueous environment which allows to study even weak photoacids due to its extraordinary good ability to stabilize a proton [6–9]. One special type of photoacids are so-called super-photoacids which are characterized by negative  $pK_a^*$  values (in water) [10–12]. This class of molecules allows the study of ESPT in various polar solvents, because the photoacids are so strong that they are able to transfer the proton to less good acceptor molecules, e.g., dimethyl sulfoxide (DMSO) [12–18]. Many studies on super-photoacids have also been carried out in solvent mixtures, for instance in water–methanol mixtures [19], water–acetonitrile mixtures [20], or water–acetone mixtures [21]. Importantly, time-resolved experiments have made it possible to follow ESPT on its actual time scale [13, 22, 23].

We focus on previously synthesized and spectroscopically characterized neutral super-photoacids derived from pyrene (8-hydroxy-1,3,6-pyrenetrisulfonate, HPTS), a pH-sensitive fluorescent dye from the group of arylsulfonates, with the modified molecules differing in their substituents at the aromatic pyrene core [14–16]. HPTS and related photoacids with pyrene centers were extensively studied by different time-resolved spectroscopic techniques in various environments [24–48] and also with regard to aspects of proton transfer mechanisms to a co-solute base [49–61]. Recently, also the ultrafast dynamics of super-photobases have been reported. [62–64]

The neutral super-photoacids exhibit electronic transitions in the VIS spectral region, thus being promising candidates to study proton transfer on the single-molecule level [65, 66] where UV excitation light typically leads to unwanted background signals. Furthermore, the compounds combine high photostability and high solubility, thus making them applicable as pH sensors in biological systems just like HPTS [67, 68]. Steady-state measurements and solvatochromic analysis revealed that intramolecular charge transfer on the photoacid side correlates best with the observed photoacidity. The present study deals with ultrafast dynamics of the strongest photoacid out of this series [14–16], namely tris(1,1,1,3,3,3-hexafluoropropan-2-yl)8-hydroxypyrene-1,3,6-trisulfonate (molecular structure sketched in Fig. 1c), which exhibits a high fluorescence quantum yield (91% in DMSO) [15] and excellent photostability. Owing to the strongly electron withdrawing sulfonic ester groups, the molecule exhibits in water an increase in acidity in the excited state of eight logarithmic units, i.e., orders of magnitude, as is reflected in the reported values  $pK_a = 4.4$  and  $pK_a^* = -3.9$ , respectively [14]. Hence, ESPT is also possible in solvents which exhibit a low polarity and are rather weak hydrogen-bonding acceptors. While many photoacids do not transfer a proton to the solvent DMSO upon excitation, the system investigated here does so even in acetone [14, 15, 21]. While previous studies have shown that a complex of the photoacid with a hydrogen-bond accepting molecule as well as a hydrogen-bonded ion pair have to be taken into account as intermediates to describe the emission dynamics conclusively [21, 69, 70], these intermediates are not identified in neat acetone; rather, analysis of emission data in neat acetone pointed towards solvation dynamics on the ps time scale and ESPT described by basically one time constant [21]. Here, we extend the time-resolved studies of this particularly strong super-photoacid to unravel the ultrafast dynamics in the aprotic solvent acetone by combining time-correlated single-photon counting (TCSPC) and femtosecond transient absorption (fsTA) data. In-depth analysis allows a conclusive description and an illustrative modeling within a reaction scheme considering proton-transfer dynamics in the ground and excited state.

## 2 Materials and methods

### 2.1 Sample preparation and basic spectroscopic characterization

The synthesis of tris(1,1,1,3,3,3-hexafluoropropan-2-yl)8-hydroxypyrene-1,3,6-trisulfonate and of the methylated analogue was performed according to References [14, 15]. For sample preparation, acetone (anhydrous and of spectrophotometric grade) and trifluoroacetic acid (TFA, 99%) were used as received. For the measurement of linear absorption spectra, a JASCO V-770 spectrophotometer was used. Absorption spectra shown in Fig. 1b were recorded in situ

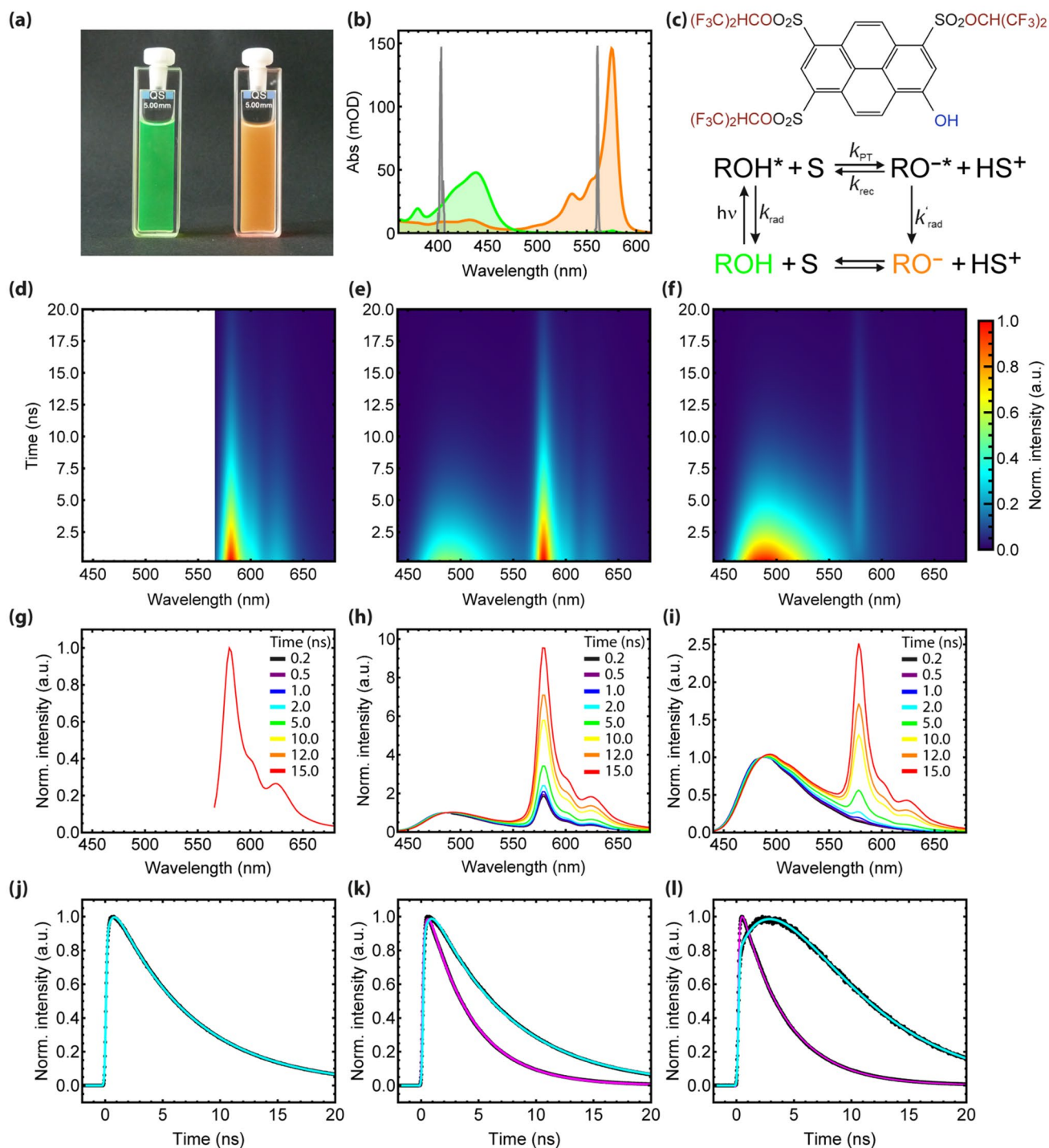


**Fig. 1** Fluorescence dynamics of the examined super-photoacid in acetone environment for two different acid-base equilibria. **a** Photograph of a neutral (orange) and an acidic (green) solution of the photoacid. **b** Absorption spectra of the neutral (orange) and acidic solution (green) used in the TCSPC experiments (note that spectra are corrected for solvent contributions). In addition, the emission spectra of the excitation laser diodes are indicated in gray. **c** Molecular structure of the investigated photoacid, with sulfonic ester moieties in red and hydroxyl group in blue, below, the one-step model used for fitting

to the data. TCSPC data is displayed for: **d** neutral solution, excited at 561 nm; **e** neutral solution, excited at 405 nm; **f** acidic solution, excited at 405 nm. **g–i** Time-resolved emission spectra taken from graphs **d–f**. The spectra are normalized to the emission at 576 nm in the case of **g** or to the emission at 486 nm in the case of **h** and **i**, respectively; note that the individual curves in **g** are coinciding within experimental error. **j–l** Normalized temporal emission profiles at 480 nm (black, fit shown in magenta) and 576 nm (black, fit shown in cyan) taken from graphs **d–f**

in a 2 mm Suprasil cuvette before acquiring TCSPC data (see below).

## 2.2 Time-correlated single-photon counting (TCSPC)

Fluorescence lifetimes of the ROH\* and RO<sup>-</sup>\* form were measured by TCSPC under magic-angle conditions [71, 72] in 90° geometry with a commercial setup (FluoTime 200 with a TimeHarp 260 correlation unit and a PMA-C-182-M photomultiplier detector assembly, Picoquant). For excitation, either a 405 nm (LDH-P-C-405) or a 561 nm (LDH-D-TA-560) pulsed diode laser (driven by a PDL-800-B oscillator module; Picoquant) was used at a repetition rate of 10 MHz. The optical density along the excitation path of the samples was well below 0.15 in order to minimize re-absorption of fluorescence photons. The instrument response function (IRF) was recorded by replacing the sample with a Ludox suspension revealing an overall time resolution of ca. 300 ps (FWHM) for both excitation wavelengths. Spectra were recorded in a cuvette with a pathlength of 2 mm. Lifetimes were determined using a custom-built Matlab fitting routine, taking into account the instrument response function and background.

## 2.3 Transient absorption spectroscopy

A regenerative Titanium:Sapphire (Ti:Sa) amplifier (Spitfire Ace; Spectra Physics: 1 kHz, 800 nm, 100 fs) was used to pump a commercial noncollinear optical parametric amplifier (NOPA, TOPAS White; Light Conversion). To selectively excite the ROH or the RO<sup>-</sup> form of the photoacid, the latter was tuned to generate 445 nm or 575 nm pump pulses having energies of 500 nJ or 350 nJ at the sample position, respectively. Supercontinuum probe pulses were generated in a linearly moving CaF<sub>2</sub> plate and used with polarization under magic angle (54.7°) with respect to the one of the pump pulses. Recording changes in optical density from pairs of subsequent laser shots was enabled by using a grating spectrograph (Acton SP2500i; Princeton Instruments) combined with a two-dimensional CCD camera (Pixis 2 K; Princeton Instruments) with an acquisition rate of 1 kHz and mechanically chopping every second pump pulse [73, 74]. When pumping at 445 nm, different absorbances of the investigated solutions were considered by globally scaling the dataset of the neutral solution with respect to the strength of the ground-state bleach signal observed for the acidic solution at 445 nm immediately after time zero. For measurements of anisotropy, a similar fsTA setup based on a Ti:Sa amplifier (Libra; Coherent: 1 kHz, 800 nm, 100 fs) was employed, using a collinear optical parametric amplifier (OPA, TOPAS-800-fs; Light Conversion) pumped at 800 nm as pump source and CaF<sub>2</sub> (5 mm) supercontinuum pumped

at 800 nm as probe source. Two complementary high-speed spectrographs (EB Stresing) for signal and reference recording were used. Pump and probe polarizations were set to 0°, 54.7°, and 90°, respectively. Here, the pump energies at the sample position were 250 nJ or 400 nJ when using 405 nm or 575 nm, respectively.

The chirp of the supercontinuum probe was removed from fsTA data [71]. Due to high photostability and the characteristic time scales, exchanging the sample volume between subsequent pump pulses was not necessary. Hence, fsTA data were recorded in a sample cell with fixed volume (Suprasil, 200 μm or 1 mm path length). Photostability was verified by recording linear absorption spectra before and after the fsTA experiment without observing any change.

## 3 Results

For disclosing the ultrafast reaction dynamics, the photoacid is investigated with TCSPC and fsTA. With each technique, two solutions with differing ground-state equilibria are examined, whereby significantly lower sample concentrations are chosen for the TCSPC measurements to avoid re-absorption of fluorescence photons. For simplicity, the solutions are called “neutral” (without TFA, orange) or “acidic” (with additional TFA, green) in the following (see also Fig. 1a). To avoid confusion, we note that the neutral form of the photoacid predominates in the case of the “acidic” sample, because the nomenclature refers to the additional acidification of the solution.

### 3.1 TCSPC

The results from our TCSPC experiments are summarized in Fig. 1. The absorption spectra shown in Fig. 1b illustrate that acidification via addition of TFA shifts the photoacid's ground-state equilibrium from the RO<sup>-</sup> form (575 nm) towards the ROH form (445 nm). In other words, one observes a transition from a mainly deprotonated ensemble of ground state molecules (orange curve) to the ensemble of fully protonated molecules in the ground state (green curve). Both neutral and acidic solutions are studied upon excitation with 405 nm light, the former is furthermore studied with 561 nm excitation. For modeling the experimental findings, we use a simplified rate model based on the Förster cycle (Fig. 1c), in which both ROH and RO<sup>-</sup> can be directly excited. The model accounts for ROH\* which either relaxes towards the ROH state with rate  $k_{\text{rad}}$  or transfers a proton with rate  $k_{\text{PT}}$  leading to RO<sup>-</sup>\* molecules which eventually can relax towards the RO<sup>-</sup> form with rate  $k'_{\text{rad}}$ . RO<sup>-</sup>\* can also be formed directly by excitation of RO<sup>-</sup> and decays back to the ground-state with  $k'_{\text{rad}}$  as well. The individual populations right after excitation depend on both the pump

wavelength and the sample under study. Geminate recombination (rate  $k_{\text{rec}}$ ) is omitted, the occurrence of ESPT is therefore reflected in the dynamics with rate  $k_{\text{rad}} + k_{\text{PT}}$ .

By illuminating the neutral solution with 561 nm light, only the  $\text{RO}^-$  form is excited. The corresponding fluorescence originating solely from  $\text{RO}^-$  is recorded from 568 to 700 nm (Fig. 1d). When normalizing these time-resolved emission spectra (Fig. 1g), they exhibit an identical shape. Hence, there are no spectral shifts and identical dynamics are observed for all emission wavelengths, exemplarily shown in Fig. 1j for 576 nm. A mono-exponential fit to these data already yields a good agreement (adjusted  $R^2 = 0.9982$ ). However, best results are obtained when an additional sub-ns exponential component is included (adjusted  $R^2 = 0.9999$ ). While this is at the limit of the temporal resolution of the TCSPC device, it indicates that there are short-lived dynamics taking place as well, entailing subsequent investigations with fsTA (vide infra). For the ns decay time, a time constant of  $k'_{\text{rad}}{}^{-1} = 6.9$  ns is found.

Figures 1e, f display the fluorescence dynamics obtained after exciting the neutral or acidic solution with 405 nm light, respectively. Under these conditions, the excitation additionally confirms the existence of  $\text{ROH}^*$  as a fluorescent species, whereby the anion's fluorescence (575 nm) is shifted towards longer wavelengths compared to the free photoacid (emitting in the spectral region around 480 nm). Again, the data are also visualized by time-resolved emission spectra (Fig. 1h, i), this time after normalizing each individual spectrum to the  $\text{ROH}^*$  fluorescence at 486 nm. A comparison of these spectral profiles discloses that the  $\text{ROH}^*$  fluorescence signal is higher relative to the one of  $\text{RO}^-$  when using a solution with a higher degree of acidification [21]. The normalized representation reveals that the emission in the region around 480 nm slightly red-shifts with time. On the one hand, this originates from the superposition with the  $\text{RO}^-$  emission and possible solvent rearrangement. On the other hand, the data of Fig. 1h, i also indicate the presence of ion-pair signals, since emission from ion pairs which have not separated completely usually appears in the spectral region around 550 nm for this photoacid (as e.g. observed in previous studies with water admixtures [21]), however, an identification of the involved cation is not possible from the data.

For both solutions under 405 nm excitation, the  $\text{ROH}^*$  fluorescence signal appears within the time resolution of the experimental apparatus and decays in a mono-exponential manner with a time constant of 4.0 ns, as is evident from the emission at 486 nm (black data with magenta fit in Fig. 1k, l, adjusted  $R^2 = 0.9983$  and 0.9995, respectively). Noteworthy, due to matching time constants for both solutions, putative traces of water seem negligible, as additional water has a more severe effect on the dynamics in neutral than in acidic solution [21]. In contrast, the temporal profiles associated

with the  $\text{RO}^-$  emission monitored at 576 nm (cyan curves) are not identical (Fig. 1k, l). The total amount of fluorescing deprotonated molecules  $[\text{RO}^-](t)$  is given by the contributions of excited deprotonated molecules, which are formed by ESPT from  $\text{ROH}^*$  ( $[\text{RO}^-]_{\text{ESPT}}$ ), and of directly excited  $\text{RO}^-$  molecules ( $[\text{RO}^-]_{\text{direct}}$ ):

$$[\text{RO}^-](t) = \frac{[\text{RO}^-]_{\text{ESPT}}(k_{\text{rad}} + k_{\text{PT}})}{(k_{\text{rad}} + k_{\text{PT}}) - k'_{\text{rad}}} \left( -e^{-(k_{\text{rad}} + k_{\text{PT}})t} + e^{-k'_{\text{rad}}t} \right) + [\text{RO}^-]_{\text{direct}} e^{-k'_{\text{rad}}t}$$

where the rate constants correspond to those from Fig. 1c (with  $k_{\text{rec}}$  set to zero). The first term thus describes a contribution that exhibits an exponential rise time  $\tau = (k_{\text{rad}} + k_{\text{PT}})^{-1} \approx 4.0$  ns and a subsequent exponential decay with  $k'_{\text{rad}}{}^{-1}$ , whereas the second term describes a direct exponential decay with  $k'_{\text{rad}}{}^{-1}$ , resembling the direct  $\text{RO}^-$  emission displayed in Fig. 1j with  $k'_{\text{rad}}{}^{-1} = 6.9$  ns. The ratio  $x = [\text{RO}^-]_{\text{ESPT}} / [\text{RO}^-]_{\text{direct}}$  of these two contributions, determined with the same fit model comprising fixed values of  $(k_{\text{rad}} + k_{\text{PT}})^{-1} = 4.0$  ns and  $k'_{\text{rad}}{}^{-1} = 6.9$  ns, is different for the data measured in neutral (Fig. 1k,  $x = 0.08$ , adjusted  $R^2 = 0.9985$ ) and acidic (Fig. 1l,  $x = 1.44$ , adjusted  $R^2 = 0.9995$ ) solution, respectively, as a consequence of the different initial concentrations of  $\text{ROH}$  or  $\text{RO}^-$  in the two samples.

### 3.2 Transient absorption

The fsTA of the neutral solution after selective excitation of the  $\text{RO}^-$  form with pulses spectrally centered at 575 nm is displayed in Fig. 2a. We observe negative signatures around 575 nm originating from the ground-state bleach (GSB) of the  $\text{RO}^-$  absorption as well as stimulated emission (SE) of the  $\text{RO}^-$  form, and a positive signature centered around 450 nm reflecting the excited-state absorption (ESA) of the  $\text{RO}^-$  form. All signals are formed directly after time zero and decay with identical time constants. Importantly, the observed dynamics do not contain any spectral signatures of the  $\text{ROH}$  form, hence the excitable  $\text{RO}^-$  are not in close proximity to a molecule that could transfer a proton (as, e.g., in the case of contact ion pairs in the electronic ground state).

Figure 2c illustrates the fsTA of the acidic solution after excitation at 445 nm. Negative signals originating from the GSB of the  $\text{ROH}$  absorption between 375 and 450 nm are observed, as well as two positive signatures appearing at 340 nm and 470 nm reflecting the ESA of the  $\text{ROH}^*$  form (for a discourse on the latter signal, see Subsection “*Approach to Disassemble the fsTA Data*”). Since we do not observe any GSB signal at 575 nm directly after the pump interaction, we can infer that only the  $\text{ROH}$  form is excited

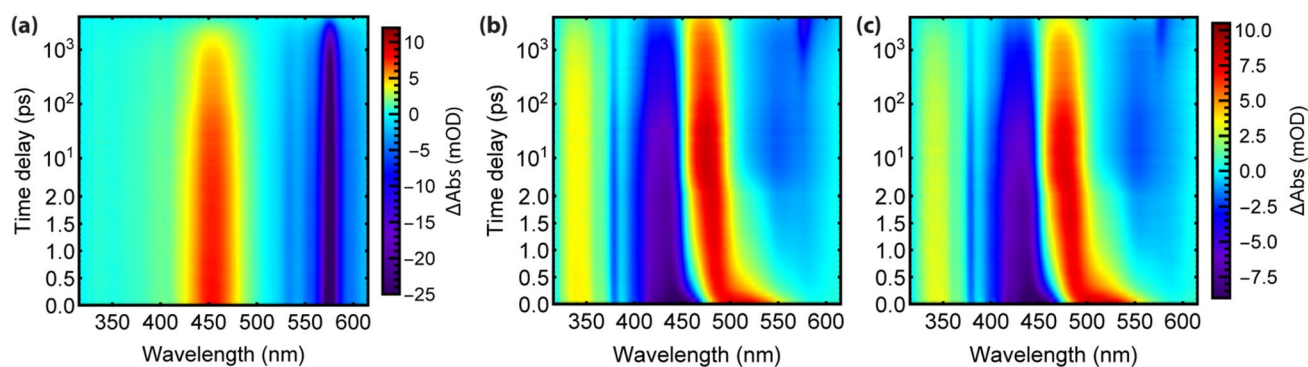


**Fig. 2** Transient absorption of the super-photoacid in acetone environment for two different acid-base equilibria. Data from fsTA experiments are shown for a pump–probe delay range of 4 ns; note the lin-log time axis (linear up to 2 ps, logarithmic afterwards) chosen to better visualize the characteristic time scales. **a** Neutral solu-

tion, excited at 575 nm; **b** neutral solution, excited at 445 nm; **c** acidic solution, excited at 445 nm [note that **b** and **c** have the same color scale]. The photoacid concentration was 616  $\mu\text{M}$ , with 2 mM TFA added for **c**. The maximum optical density of the sample was 0.4

in this measurement. As observed in Fig. 2a when exciting the base form only, both ESA and GSB signals are formed directly after time zero and decay on the same time scale. Within the first few picoseconds, spectral shifts imprinted in the ESA signal and the GSB are present, after which a negative signal is observable around 550 nm. After several hundreds of picoseconds, a pronounced negative signal at 575 nm appears, and the ESA signal around 470 nm exhibits a blue shift on the same timescale. These dynamics evidence ESPT, as will be outlined below.

Figure 2b shows the fsTA of the neutral solution after exciting the non-dissociated ROH molecules, addressing the proton-transfer dynamics of the photoacid from a different ground-state equilibrium. At first glance, only minor differences compared to Fig. 2c appear, and hence we can infer that under neutral conditions mainly ROH rather than RO<sup>−</sup> is excited at 445 nm.

Generally, a global analysis [75] of photodynamic processes can be performed, with an exponential ansatz resulting in decay-associated difference spectra (DADS). If done for our data, the contributions in the ns regime resemble the findings in the TCSPC study (Fig. 1d). However, the dynamics for 445 nm excitation of both neutral and acidic solutions (Fig. 2b, c) exhibit pronounced spectral shifts during the first 100 ps. As the transient spectra themselves show a temporal behavior on these short timescales, global analysis with an exponential ansatz can only approximately describe these dynamics, giving rise to additional derivative-like DADS [76–80]. Recent studies have reported different advanced approaches to include spectral shifts in global analysis [81–84], however, we refrain from an analysis of DADS here and rather follow an alternative route to disentangle the dynamics, as outlined below.

## 4 Analysis and discussion

### 4.1 Dynamics after RO<sup>−</sup> excitation

When exciting the RO<sup>−</sup> form directly, no signature of the protonated solute is found, hence we infer that all transient absorption and emission signals originate from the deprotonated form. Specifically, we do not observe any indication of a re-protonation process. Besides energetic limitations, one would need to rationalize how a proton could approach an RO<sup>−</sup>\* anion after the photoexcitation. The following three scenarios all are unlikely for different reasons: (1) a proton is transferred from a methyl group of acetone; (2) a proton or a protonated acetone reaches the RO<sup>−</sup>\* (present for only a few ns) in a diffusion-controlled process; (3) ground-state ion pairs are present in solution, i.e., a RO<sup>−</sup> solute is not shielded by a solvent shell from a protonated acetone cation.

In the TCSPC data (Fig. 1d, g), the spectral shape does not change with time. Globally fitting the fsTA data yields a fast component (0.9 ps, see Fig. 3a) with which minor spectral shifts of a few nm are associated. We assign this behavior to solvation dynamics of the acetone environment as a reaction to the change in charge distribution in the solute upon photoexcitation. Maroncelli and coworkers report non-specific solvation dynamics of acetone to exhibit decay times of 0.187 ps and 1.09 ps; [85] while we could not explicitly deduce the former one, we identify them to correspond to the fastest time scale deduced from the fsTA data.

Steady-state spectra of RO<sup>−</sup> exhibit almost no significant Stokes shift in any solvent, indicating that predominantly the  $v' = 0 \leftarrow v'' = 0$  vibronic transition is excited, but also that the reorganization energy for the solvation process must be small [85–87]. This implies that the solvation shells of

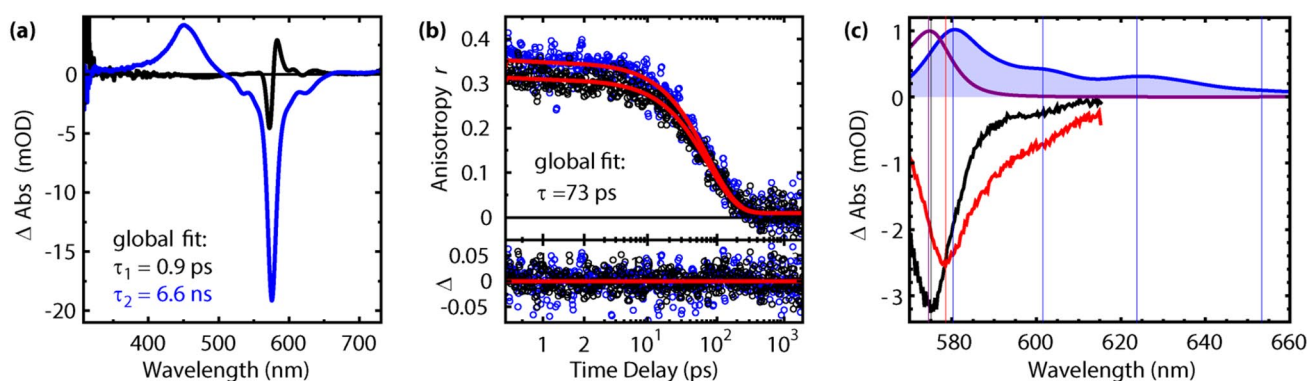


**Fig. 3** **a** Example of decay-associated difference spectra from global analysis of a fsTA data set of the super-photoacid in neutral acetonous solution for 575 nm excitation, i.e., exciting  $\text{RO}^-$ . **b** Temporal decay of the anisotropy in the ESA (black, probe wavelength 450 nm) and SE/GSB region (blue, probe wavelength 580 nm) of  $\text{RO}^{*-}$ ; note the logarithmic abscissa and the residuals as a measure of the fit

the  $\text{RO}^-$  and the  $\text{RO}^{*-}$  form are similar or at least that the rearrangement is not connected to large energetic changes, as can be rationalized since both the ground-state and the excited-state species are anionic.

HPTS and derivatives can exhibit a pronounced vibronic progression both in the absorption and the emission spectrum and both in the protonated and deprotonated form. Clear vibronic signatures are found in solvents with a low ability to donate a hydrogen bond, whereas the spectra are basically structureless if the solvent is a good hydrogen-bond donor [88]. In the low-energy part of the electronic absorption spectrum, two electronic states contribute which can mix significantly and may contribute differently to the vibronic structure [88]. In our data (Fig. 1d, g, and 2a), the decay dynamics (excluding the sub-100 ps contribution associated with solvation) are identical and mono-exponential with a time constant of around 6.9 ns for all emission/probe wavelengths (Fig. 3a).

Repetition of the experiments with different polarization conditions for the pump and probe beams has indicated further dynamics on the order of several tens of picoseconds. This behavior points towards rotational diffusion of the super-photoacid in the acetonous environment. To clarify this point, measurements with parallel [signal intensity  $I_{||}(t)$ ] and perpendicular [ $I_{\perp}(t)$ ] pump and probe polarization directions have been performed and the anisotropy [72, 75, 89–98]

$$r(t) = \frac{I_{||}(t) - I_{\perp}(t)}{I_{||}(t) + 2I_{\perp}(t)}$$

was derived for the full spectral range covering all features. A global mono-exponential fit to the anisotropy data describes these sufficiently well with an optimized decay

quality. **c** Transient spectra at 4 ns pump-probe delay for the neutral solution after excitation at 575 nm (black) or 445 nm (red). For comparison, the SE profile of  $\text{RO}^{*-}$  is shown in blue and the absorption spectrum of  $\text{RO}^-$  is shown in purple. Vertical lines indicate the spectral positions of the maxima

time constant of 73 ps (see transient anisotropy data at two exemplary probe wavelengths in Fig. 3b). This time constant is assigned to rotational diffusion, and under the approximation of a spherical solute (which is a simplification, but for instance an oblate rotor would already give rise to biexponential rotational behavior) [90] leads to an estimation of a molecular diameter of roughly 1.2 nm.

## 4.2 Population dynamics of $\text{ROH}^*$

The emission signal of the excited photoacid  $\text{ROH}^*$  observed at 480 nm (Fig. 1k, l) exhibits a mono-exponential decay with a time constant of 4.0 ns. Specifically, we do not observe a non-exponential contribution which would be characteristic of an excited-state geminate recombination process, i.e., that the proton is transferred to an acetone molecule but can come back to form  $\text{ROH}^*$  again [16, 24, 25]. We thus omit the occurrence of excited-state geminate recombination and conclude that  $\text{ROH}^*$  is depopulated with an overall rate  $k_{\text{rad}} + k_{\text{PT}} = (4.0 \text{ ns})^{-1}$  in acetonous environment. The fsTA data (Fig. 2b, c) contains this information as well, further reflected not only in the SE but also in the ESA dynamics. The depopulation of  $\text{ROH}^*$  is thus much slower than in water (ca. 3 ps) [16], methanol (0.12 ns) [16], ethanol (0.2 ns) [16], or DMSO (0.8 ns) [15], as a consequence of the reduced excited-state acidity in acetone, which is the reason why many photoacids will not perform an ESPT in acetone at all.

## 4.3 Differences in the $\text{RO}^-$ spectral region depending on pumped species

The pump wavelength determines which species are excited, but due to the ESPT, also the emergence of newly formed

transient signals depends on the excitation. We focus on the fsTA data in the spectral region from 560 to 700 nm and juxtapose in Fig. 3c the difference spectra for a time delay of 4 ns extracted from Fig. 2a, b to the steady-state absorption of RO<sup>-</sup> and the emission of RO<sup>-\*</sup> (converted from fluorescence to stimulated emission).

For the case of the neutral solution excited with 575 nm, no contribution from ROH\* is expected and the difference spectrum (black curve in Fig. 3c) comprises both GSB of RO<sup>-</sup> and SE of RO<sup>-\*</sup>. Hence, the spectral peak position is not at the maximum emission wavelength of 575 nm but lower due to the GSB contribution. If the same solution is excited with 445 nm, the predominant signal originates from RO<sup>-\*</sup> molecules that were formed from ROH\* by ESPT. These RO<sup>-\*</sup> molecules contribute an SE signal but no GSB signal. By contrast, when already relaxed to the ground state, a positive absorption caused by these newly formed RO<sup>-</sup> molecules is added, partially canceling the blue edge of the SE of the RO<sup>-\*</sup> molecules. Hence, the peak in the difference spectrum (red curve in Fig. 3c) is positioned further to the red and closer to the maximum of the RO<sup>-\*</sup> emission (blue curve in Fig. 3c). Furthermore, there is also a broad underlying contribution of SE from ROH\* molecules reaching out to this spectral regime (compare Fig. 1b and Reference [21]).

#### 4.4 Comparison to a methylated analogue

For assignment of the different signal contributions, it is advantageous to also study the methylated analogue tris(1,1,1,3,3,3-hexafluoropropan-2-yl)8-methoxypyrene-1,3,6-trisulfonate, i.e., where the hydroxy group is replaced by a methoxy group and therefore no ESPT is possible.

Figure 4 shows the corresponding fsTA data, together with the temporal decay of the anisotropy and the quantum-chemically geometry-optimized structure. Besides solvation dynamics within the first few ps, long-lived signals are observed. The GSB is accompanied by two ESA signals, one at lower (ca. 350 nm) and one at higher (ca. 550 nm) wavelengths. These signals are analogous to those for ROH\* in Fig. 2b, c, and the measurements corroborate that the latter are not related to any ESPT process. Nonetheless, also since the spectral positions of absorption and emission are blue-shifted for ROME compared to ROH [21], the spectral position of the low-frequency ESA signal differs for ROH\* and ROME\*, being centered towards 550 nm for ROME\* but below 500 nm for ROH\* (see next section). Furthermore, a mono-exponential fit to the anisotropy data for ROME\* (Fig. 4b) yields a rotational diffusion time of 68 ps that matches within error the 73 ps obtained for RO<sup>-\*</sup> (Fig. 3b). We note that the slight difference might be associated with RO<sup>-\*</sup> being anionic, whereas ROME\* is not. Thus, we conclude that ROME\* and RO<sup>-\*</sup> (and probably also ROH\*, for which anisotropy was not explicitly measured) behave alike in a fashion similar to a spherical rotor (Fig. 4c). In particular, for the case of RO<sup>-\*</sup>, no indications for a strongly bound counter ion or a solvent shell rotating with the solute are found.

#### 4.5 Approach to disassemble the fsTA data

If several different species are involved and solvation is pronounced, global analysis is tedious and comprises several derivative-like features (as the black curve in Fig. 3a) to mimic spectral shifts [76–80]. Thus, instead of a global fit to the fsTA data for ROH excitation, we here do not want to

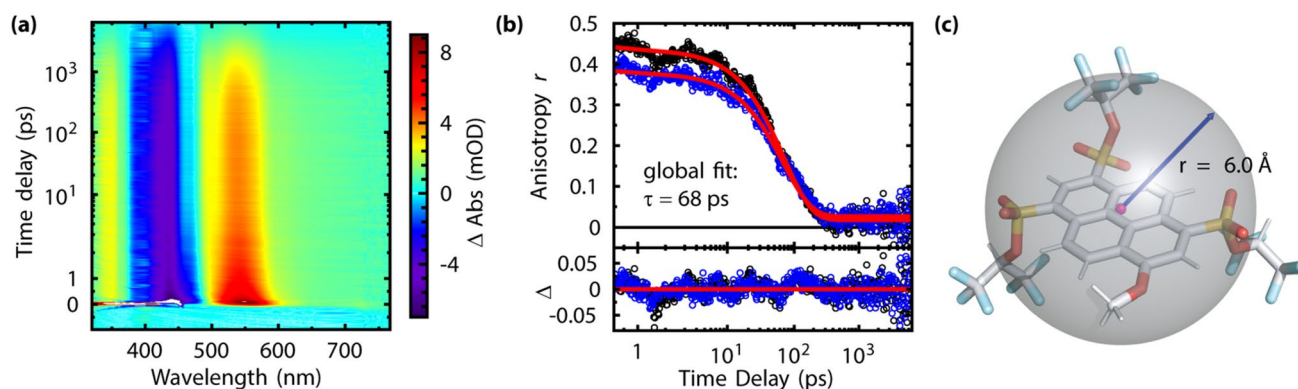


**Fig. 4** Studies for the methylated analogue ROME [structure in panel c] in (neutral) acetone solution for 405 nm excitation. **a** Data from fsTA experiments; note the lin-log time axis (linear up to 2 ps, logarithmic afterwards) chosen to better visualize the characteristic time scales. **b** Temporal decay of the anisotropy in the ESA (blue, probe wavelength 548 nm) and SE/GSB region (black, probe wavelength 427 nm) of ROME\*<sup>\*</sup>; note the logarithmic abscissa and the residuals

as a measure of the fit quality. **c** Geometry of ROME, quantum-chemically optimized at the semi-empirical AM1 level of theory (carbons in grey, hydrogens in white, oxygens in red, sulfurs in yellow and fluorines in cyan). A sphere with a diameter of 1.2 nm, as deduced from the rotational diffusion time under the assumption of a spherical rotor, is plotted for comparison



fit but rather to reconstruct it systematically by separately addressing the different signal components and subsequently adding them up. For this, we have to identify how many components contribute and what the associated time scales and underlying processes (ESPT, solvation shift, ground-state refilling, etc.) are.

In the scheme derived from the original Förster cycle that we will also use here, there are just two excited-state species,  $\text{ROH}^*$  and  $\text{RO}^{*-}$ , and the corresponding ground-state species,  $\text{ROH}$  and  $\text{RO}^-$ , respectively (Fig. 1c). To describe ESPT, population can go directly from  $\text{ROH}^*$  to  $\text{RO}^{*-}$  with a characteristic rate. In literature, this picture was extended in analogy to the Eigen-Weller reaction scheme for bimolecular acid-base reactions to involve a contact ion pair, produced by an initial short-range proton transfer and composed of  $\text{RO}^{*-}$  and the dissociated proton in close proximity. Only in a second step, the ions separate via diffusion, which is why this model is called two-step model. Huppert and coworkers [32, 33] further augmented the two-step model by including an additional intermediate of the diffusive separation, a solvent-separated ion pair which is formed if only few solvent molecules have inserted in between the ions, still being held together by Coulombic interactions. Furthermore, if the photoacid and the proton acceptor are not in direct proximity prior to excitation, the (diffusive) formation of an encounter complex will constitute the first step. These models could well describe rather fast ESPT processes, and the individual intermediates could be identified in several experiments.

Here, we know that the photoacid under investigation is only of moderate strength in acetone and that ESPT occurs on the nanosecond time scale. Our previous study has clearly revealed the existence of complexes and hydrogen-bonded ion pairs with water molecules in the case of binary solvent environments of acetone and water, but also showed the distinctly different behavior for neat acetone [21]. Hence, we do not explicitly consider the ion separation step, nor do we have to take geminate recombination into account, as is corroborated by a mono-exponential emission decay rather than a non-exponential behavior [25]. Proton-induced quenching, as observed for instance in naphthols as another non-radiative process [10, 12, 22, 99–102], is unlikely to occur in the investigated system since the solvent is aprotic and the solute could only be quenched by a proton it has just transferred, a process that seems unlikely if even geminate recombination is marginal, an interpretation also supported by the high fluorescence yield. [15]

For modeling the fsTA of Fig. 2c, we thus take the model of Fig. 1c and identify six spectral contributions: the GSB of the  $\text{ROH}$  form ( $\text{RO}^-$  is not present and hence not directly excited), the ESA and SE signals of  $\text{ROH}^*$  and of  $\text{RO}^{*-}$  formed after ESPT, respectively, and the  $\text{RO}^-$  ground-state absorption (GSA) from molecules formed from  $\text{ROH}$  via the ESPT pathway. In addition, the solvation shift is included

by the characteristic time constants (0.187 ps and 1.09 ps) and relative amplitudes (0.565 and 0.435) reported in Reference [85].

We derive the individual absorption spectral profiles from the steady-state data (Fig. 1b), ESA signals are estimated from the fsTA data sets and approximated by Gaussians. As is known for pyranine and also evident from the data in Fig. 2, the ESA of the  $\text{RO}^{*-}$  is blue-shifted relative to the major ESA signal of  $\text{ROH}^*$  [37, 44]. For the spectral SE profiles of the  $\text{ROH}^*$  and  $\text{RO}^{*-}$  form, respectively, the emission spectrum after exciting  $\text{ROH}$  in an acidic solution is first interpolated, then divided into contributions from the  $\text{ROH}^*$  and  $\text{RO}^{*-}$  form by subtracting, after reasonable rescaling, the spectrum of the base form excited at 561 nm (Fig. 1g), and finally transferred from fluorescence to SE profiles by applying the  $\lambda^4$  correction related to the differences in the corresponding Einstein coefficients [103, 104]. These normalized spectral profiles are displayed in Fig. 5a. Importantly, these spectra are shown prior to putative spectral shifts, hence we assume that the spectral profile of the components does not change but spectrally shifts and grows/decreases with time. As a consequence, the SE signal of  $\text{ROH}^*$  is shown with its maximum at the  $\text{ROH}$  absorption around 440 nm, i.e., mimicking SE from the Franck-Condon point directly after excitation, which will shift towards the center of the static  $\text{ROH}^*$  fluorescence at 488 nm with the parameters of the solvation process. The same holds for the red-edge ESA signal which undergoes a solvation shift (in contrast to the blue-edge ESA or the ESA of the  $\text{RO}^{*-}$ , compare Fig. 2 and discussion below). The GSB dynamics remaining beyond the temporal window of the fsTA setup are estimated from the decay constant of the ESA of  $\text{ROH}^*$  and the emission lifetime of  $\text{ROME}^*$  [21]. With the spectral profiles and determined time scales fixed, the amplitudes of the components are adjusted so that the fsTA data is adequately reproduced. The result is shown in Fig. 5, with the sum of all components (Fig. 5h) being in good accordance with the experiment (Fig. 2c, again plotted in Fig. 5i to allow a direct comparison).

While the spectral signatures of the individual components are already quite well separated for the super-photoacid, the advantage of this approach is that one can plot each contribution individually, as is done in panels b to g of Fig. 5. The analysis shows that the ESA and the SE of  $\text{ROH}^*$  overlap and shift in opposite directions, as also reported for HPTA [30]. The shifts here are so pronounced that the two bands “shift through” each other, i.e. initially after excitation, SE is at shorter wavelengths than ESA, while it is the opposite on long time scales. After several nanoseconds, the signatures of  $\text{RO}^{*-}$  grow in, leading to the observed overall blue-shift of ESA in the spectral region 450–500 nm. In the spectral region above 560 nm, a decreasing SE signal of  $\text{ROH}^*$  and a rising one from  $\text{RO}^{*-}$  contribute, overlapped

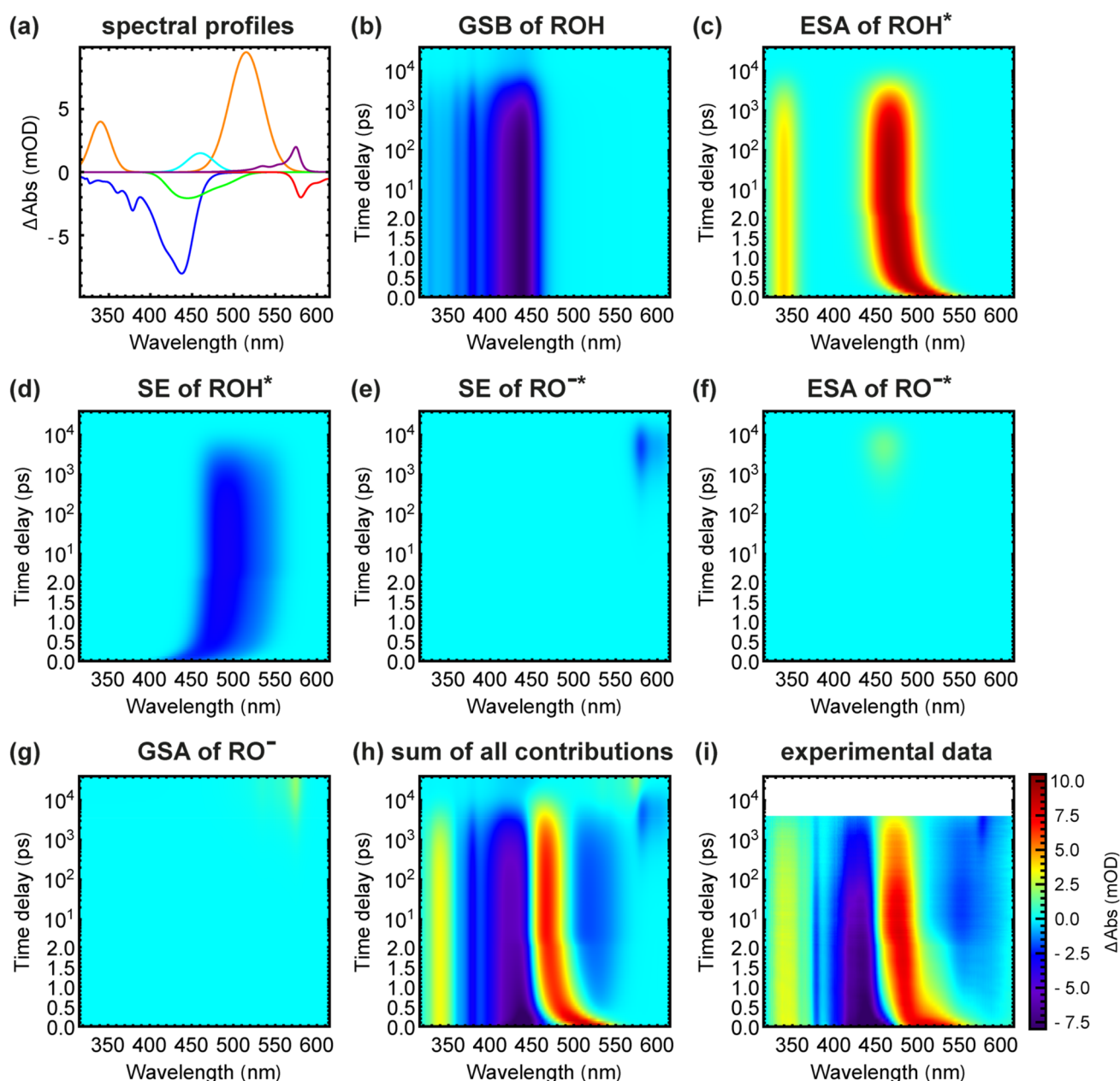


**Fig. 5** Modeling the fsTA data shown in Fig. 2c. **a** Individual spectral profiles comprising the GSB of ROH (blue), the ESA of ROH\* (orange), the ESA of RO<sup>-\*</sup> (cyan), the SE of ROH\* (green), the SE of RO<sup>-\*</sup> (red), and the GSA of RO<sup>-</sup> (purple). **b** GSB of ROH; **c** ESA of ROH\*; **d** SE of ROH\*; **e** SE of RO<sup>-\*</sup>; **f** ESA of RO<sup>-\*</sup>; **g** GSA of RO<sup>-</sup> (assuming re-protonation of RO<sup>-</sup> to ROH is negligible on the

displayed time scale). **h** Modeled transient absorption data combining individual transient features shown in (b-g). **i** Experimental data from Fig. 2c for comparison. Note that the simulations go out to 40 ns, while the fsTA experiment only goes to 4 ns; the time delay axis is logarithmic from 2 ps to 40 ns

with an absorption signal of newly formed RO<sup>-</sup> molecules (which is not evident in the fsTA data of Fig. 5i as RO<sup>-\*</sup> rises with 4.0 ns and decays with 6.9 ns, but the fsTA data does not exceed delay times of 4 ns). Importantly, there is no contribution of GSB of RO<sup>-</sup>, as none of these molecules were initially present in the acidic solution (as discussed above for Fig. 3c).

The ESA of ROH\* (Fig. 5c) comprises two contributions, where only the one at the higher-wavelength shows a solvation shift. The ESA at lower wavelength behaves in analogy to the ESA of RO<sup>-\*</sup> (Fig. 3a), thus, is blue-shifted with respect to the GSB and does not show any solvation shift. From this, we conclude that the lower wavelength signal is the analogous ESA of ROH\*. The presence of

corresponding ESA signals for ROME\* (Fig. 4a) corroborates this assignment.

The agreement between the modeled (Fig. 5h) and the experimental (Fig. 5i) data suggests that the main involved species and associated signals are covered, although our approach is not a fit but rather an adjusted qualitative model, yet the occurrence of pronounced signals from putative species not considered would become apparent. Hence, we conclude that during the ESPT dynamics in acetoneous environment, no intermediate species like ion pairs emerge to a conspicuous degree or at least do not cause pronounced transient signals. As these species can be identified when small amounts of water are added to the solution [21], their absence in the here reported experimental data support ESPT to acetone to a low extent.

## 5 Conclusion

This ultrafast spectroscopy study unveils the excited-state proton-transfer dynamics of an extraordinarily strong photoacid in the aprotic solvent acetone—an environment which, due to weaker proton-transfer capabilities of other photoacids, could not be investigated in most of the existing studies on photoacidity. Direct excitation of the anion RO<sup>−</sup> revealed that there are solvation dynamics on a ps time scale which are characteristic for acetoneous environments, and rotational diffusion occurs with a time constant of about 70 ps, suggesting a diameter of the solute of 1.2 nm. Elucidation of the dynamics after ROH excitation is realized by investigating neutral and acidic acetoneous solutions of the photoacid and comparison to the methylated analogue. Since various positive and negative signals superpose in the fsTA data, a decomposition into individual signal contributions was pursued in order to unravel the contributing components. These studies corroborate the potential of this particularly strong super-photoacid to be exploited as light-triggered proton donor in experimental conditions where this is unfeasible otherwise. Future studies will address ESPT dynamics under even harsher conditions, achievable with magic photoacids [105].

**Acknowledgements** We thank PicoQuant GmbH, Berlin, for the loan of the laser diode head LDH-D-TA-560. We furthermore thank Dr. Sebastian Goetz for providing the photographic images for Figure 1a and for the artwork of the graphical abstract. Different aspects of this work were supported by the Deutsche Forschungsgemeinschaft (DFG, German Research Foundation) within the Research Training Group “Confinement-controlled Chemistry” (Grant GRK2376, Project 331085229), through Grant JU 650/8-1, and under Germany’s Excellence Strategy EXC 2033—390677874—RESOLV.

**Funding** Open Access funding enabled and organized by Projekt DEAL.

## Declarations

**Conflict of interest** The authors declare that there is no conflict of interest.

**Open Access** This article is licensed under a Creative Commons Attribution 4.0 International License, which permits use, sharing, adaptation, distribution and reproduction in any medium or format, as long as you give appropriate credit to the original author(s) and the source, provide a link to the Creative Commons licence, and indicate if changes were made. The images or other third party material in this article are included in the article’s Creative Commons licence, unless indicated otherwise in a credit line to the material. If material is not included in the article’s Creative Commons licence and your intended use is not permitted by statutory regulation or exceeds the permitted use, you will need to obtain permission directly from the copyright holder. To view a copy of this licence, visit <http://creativecommons.org/licenses/by/4.0/>.

## References

1. Trieff, N. M., & Sundheim, B. R. (1965). The effect of solvent on the acid-base kinetics of the excited state of  $\beta$ -naphthol. *The Journal of Physical Chemistry*, 69, 2044–2059.
2. Weber, K. (1931). Über die enge Beziehung der Fluoreszenzauslöschung zur Hemmung photochemischer Reaktionen. *Zeitschrift für Physikalische Chemie*, 15B, 18–44.
3. Förster, T. (1949). Fluoreszenzspektrum und Wasserstoffionenkonzentration. *Naturwissenschaften* 36, 186–187.
4. Förster, T. (1950). Elektrolytische Dissoziation angeregter Moleküle. *Zeitschrift für Elektrochemie und angewandte physikalische Chemie*, 54, 42–46.
5. Braslavsky, S. E. (2007). Glossary of terms used in photochemistry, 3rd edition (IUPAC Recommendations 2006). *Pure and Applied Chemistry*, 79, 293–465.
6. Marx, D., Tuckerman, M. E., Hutter, J., & Parrinello, M. (1999). The nature of the hydrated excess proton in water. *Nature*, 397, 601–604.
7. Agmon, N. (1999). Proton solvation and proton mobility. *Israel Journal of Chemistry*, 39, 493–502.
8. Kornyshev, A. A., Kuznetsov, A. M., Spohr, E., & Ulstrup, J. (2003). Kinetics of proton transport in water. *The Journal of Physical Chemistry B*, 107, 3351–3366.
9. Knight, C., & Voth, G. A. (2012). The curious case of the hydrated proton. *Accounts of Chemical Research*, 45, 101–109.
10. Solntsev, K. M., Huppert, D., & Agmon, N. (1999). Photochemistry of “super”-photoacids. Solvent effects. *The Journal of Physical Chemistry A*, 103, 6984–6997.
11. Simkovitch, R., Shomer, S., Gepshtein, R., & Huppert, D. (2015). How fast can a proton-transfer reaction be beyond the solvent-control limit? *The Journal of Physical Chemistry B*, 119, 2253–2262.
12. Tolbert, L. M., & Solntsev, K. M. (2002). Excited-state proton transfer: From constrained systems to “super” photoacids to superfast proton transfer. *Accounts of Chemical Research*, 35, 19–27.
13. Simkovitch, R., et al. (2013). Ultrafast excited-state proton transfer from hydroxycoumarin-dipicolinium cyanine dyes. *Journal of Photochemistry and Photobiology A: Chemistry*, 254, 45–53.
14. Spies, C., Finkler, B., Acar, N., & Jung, G. (2013). Solvatochromism of pyranine-derived photoacids. *Physical Chemistry Chemical Physics*, 15, 19893–19905.

15. Finkler, B., et al. (2014). Highly photostable “super”-photoacids for ultrasensitive fluorescence spectroscopy. *Photochemical & Photobiological Sciences*, *13*, 548–562.
16. Spies, C., et al. (2014). Solvent dependence of excited-state proton transfer from pyranine-derived photoacids. *Physical Chemistry Chemical Physics*, *16*, 9104–9114.
17. Kumpulainen, T., Rosspeintner, A., Dereka, B., & Vauthey, E. (2017). Influence of solvent relaxation on ultrafast excited-state proton transfer to solvent. *The Journal of Physical Chemistry Letters*, *8*, 4516–4521.
18. Verma, P., Rosspeintner, A., Dereka, B., Vauthey, E., & Kumpulainen, T. (2020). Broadband fluorescence reveals mechanistic differences in excited-state proton transfer to protic and aprotic solvents. *Chemical Science*, *11*, 7963–7971.
19. Solntsev, K. M., Huppert, D., Agmon, N., & Tolbert, L. M. (2020). Photochemistry of “super” photoacids. 2. Excited-state proton transfer in methanol/water mixtures. *The Journal of Physical Chemistry A*, *104*, 4658–4669.
20. Pérez-Lustres, J. L., et al. (2007). Ultrafast proton transfer to solvent: Molecularity and intermediates from solvation- and diffusion-controlled regimes. *Journal of the American Chemical Society*, *129*, 5408–5418.
21. Sülzner, N., Geissler, B., Grandjean, A., Jung, G., & Nuernberger, P. (2022). Excited-state proton transfer dynamics of a super-photoacid in acetone-water mixtures. *ChemPhotoChem*, *6*, e202200041.
22. Prémont-Schwarz, M., Barak, T., Pines, D., Nibbering, E. T. J., & Pines, E. (2013). Ultrafast excited-state proton-transfer reaction of 1-naphthol-3,6-disulfonate and several 5-substituted 1-naphthol derivatives. *The Journal of Physical Chemistry B*, *117*, 4594–4603.
23. Corani, A., et al. (2013). Excited-state proton-transfer processes of DHICA resolved: From sub-picoseconds to nanoseconds. *Journal of Physical Chemistry Letters*, *4*, 1383–1388.
24. Pines, E., & Huppert, D. (1986). Geminate recombination proton-transfer reactions. *Chemical Physics Letters*, *126*, 88–91.
25. Pines, E., Huppert, D., & Agmon, N. (1988). Geminate recombination in excited-state proton-transfer reactions: Numerical solution of the Debye-Smoluchowski equation with backreaction and comparison with experimental results. *The Journal of Chemical Physics*, *88*, 5620–5630.
26. Pines, E., & Huppert, D. (1989). Salt effect in photoacid quantum yield measurements: A demonstration of the geminate recombination role in deprotonation reactions. *Journal of the American Chemical Society*, *111*, 4096–4097.
27. Tran-Thi, T.-H., Gustavsson, T., Prayer, C., Pommeret, S., & Hynes, J. T. (2000). Primary ultrafast events preceding the photoinduced proton transfer from pyranine to water. *Chemical Physics Letters*, *329*, 421–430.
28. Tran-Thi, T.-H., Prayer, C., Millié, Ph., Uznanski, P., & Hynes, J. T. (2002). Substituent and solvent effects on the nature of the transitions of pyrenol and pyranine. Identification of an intermediate in the excited-state proton-transfer reaction. *The Journal of Physical Chemistry A*, *106*, 2244–2255.
29. Mohammed, O. F., Dreyer, J., Magnes, B.-Z., Pines, E., & Nibbering, E. T. J. (2005). Solvent-dependent photoacidity state of pyranine monitored by transient mid-infrared spectroscopy. *ChemPhysChem*, *6*, 625–636.
30. Pines, E., Pines, D., Ma, Y.-Z., & Fleming, G. R. (2004). Femtosecond pump-probe measurements of solvation by hydrogen-bonding interactions. *ChemPhysChem*, *5*, 1315–1327.
31. Mondal, S. K., et al. (2005). Excited state proton transfer of pyranine in a  $\gamma$ -cyclodextrin cavity. *Chemical Physics Letters*, *412*, 228–234.
32. Gepshtein, R., Leiderman, P., Genosar, L., & Huppert, D. (2005). Testing the three step excited state proton transfer model by the effect of an excess proton. *The Journal of Physical Chemistry A*, *109*, 9674–9684.
33. Leiderman, P., Genosar, L., & Huppert, D. (2005). Excited-state proton transfer: Indication of three steps in the dissociation and recombination process. *The Journal of Physical Chemistry A*, *109*, 5965–5977.
34. Mohammed, O. F., Pines, D., Nibbering, E. T., & Pines, E. (2007). Base-induced solvent switches in acid-base reactions. *Angewandte Chemie International Edition*, *46*, 1458–1461.
35. Spry, D. B., Goun, A., Glusac, K., Moilanen, D. E., & Fayer, M. D. (2007). Proton transport and the water environment in nafion fuel cell membranes and AOT reverse micelles. *Journal of the American Chemical Society*, *129*, 8122–8130.
36. Spry, D. B., Goun, A., & Fayer, M. D. (2007). Deprotonation dynamics and Stokes shift of pyranine (HPTS). *The Journal of Physical Chemistry A*, *111*, 230–237.
37. Spry, D. B., & Fayer, M. D. (2007). Observation of slow charge redistribution preceding excited-state proton transfer. *The Journal of Chemical Physics*, *127*, 204501.
38. Spry, D. B., & Fayer, M. D. (2008). Charge redistribution and photoacidity: Neutral versus cationic photoacids. *The Journal of Chemical Physics*, *128*, 084508.
39. Tielrooij, K. J., Cox, M. J., & Bakker, H. J. (2009). Effect of confinement on proton-transfer reactions in water nanopools. *ChemPhysChem*, *10*, 245–251.
40. Cohen, B., Martín Álvarez, C., Alarcos Carmona, N., Organero, J. A., & Douhal, A. (2011). Proton-transfer reaction dynamics within the human serum albumin protein. *The Journal of Physical Chemistry B*, *115*, 7637–7647.
41. Carmona, N. A., Cohen, B., Organero, J. A., & Douhal, A. (2012). Excited state intermolecular proton and energy transfer of 1-hydroxypyrene interacting with the human serum albumin protein. *Journal of Photochemistry and Photobiology A: Chemistry*, *234*, 3–11.
42. Wang, Y., et al. (2013). Early time excited-state structural evolution of pyranine in methanol revealed by femtosecond stimulated Raman spectroscopy. *The Journal of Physical Chemistry A*, *117*, 6024–6042.
43. Han, F., Liu, W., & Fang, C. (2013). Excited-state proton transfer of photoexcited pyranine in water observed by femtosecond stimulated Raman spectroscopy. *Chemical Physics*, *422*, 204–219.
44. Liu, W., et al. (2016). Panoramic portrait of primary molecular events preceding excited state proton transfer in water. *Chemical Science*, *7*, 5484–5494.
45. Alarcos, N., Cohen, B., & Douhal, A. (2016). A slowing down of proton motion from HPTS to water adsorbed on the MCM-41 surface. *Physical Chemistry Chemical Physics*, *18*, 2658–2671.
46. Agmon, N., et al. (2016). Protons and hydroxide ions in aqueous systems. *Chemical Reviews*, *116*, 7642–7672.
47. Hoberg, C., et al. (2021). Caught in the act: Observation of the solvent response triggered by excited-state proton transfer in real time. *ChemRxiv*. <https://doi.org/10.33774/chemrxiv-2021-60zjv>
48. Eckert, S., et al. (2022). Electronic structure changes of an aromatic amine photoacid along the Förster cycle. *Angewandte Chemie International Edition*, *67*, e202200709.
49. Pines, E., Magnes, B.-Z., Lang, M. J., & Fleming, G. R. (1997). Direct measurement of intrinsic proton transfer rates in diffusion-controlled reactions. *Chemical Physics Letters*, *281*, 413–420.
50. Genosar, L., Cohen, B., & Huppert, D. (2000). Ultrafast direct photoacid–base reaction. *The Journal of Physical Chemistry A*, *104*, 6689–6698.
51. Rini, M., Magnes, B.-Z., Pines, E., & Nibbering, E. T. J. (2003). Real-time observation of bimodal proton transfer in acid-base pairs in water. *Science*, *301*, 349–352.

52. Rini, M., Pines, D., Magnes, B.-Z., Pines, E., & Nibbering, E. T. J. (2004). Bimodal proton transfer in acid-base reactions in water. *The Journal of Chemical Physics*, *121*, 9593–9610.
53. Nibbering, E. T. J., Fidler, H., & Pines, E. (2005). Ultrafast chemistry: Using time-resolved vibrational spectroscopy for interrogation of structural dynamics. *Annual Review of Physical Chemistry*, *56*, 337–367.
54. Mohammed, O. F., Pines, D., Dreyer, J., Pines, E., & Nibbering, E. T. J. (2005). Sequential proton transfer through water bridges in acid-base reactions. *Science*, *310*, 83–86.
55. Pines, D., Nibbering, E. T. J., & Pines, E. (2007). Relaxation to equilibrium following photoacid dissociation in mineral acids and buffer solutions. *Journal of Physics: Condensed Matter*, *19*, 065134.
56. Siwick, B. J., & Bakker, H. J. (2007). On the role of water in intermolecular proton-transfer reactions. *Journal of the American Chemical Society*, *129*, 13412–13420.
57. Siwick, B. J., Cox, M. J., & Bakker, H. J. (2008). Long-range proton transfer in aqueous acid–base reactions. *The Journal of Physical Chemistry B*, *112*, 378–389.
58. Cox, M. J., & Bakker, H. J. (2008). Parallel proton transfer pathways in aqueous acid-base reactions. *The Journal of Chemical Physics*, *128*, 174501.
59. Cox, M. J., Timmer, R. L. A., Bakker, H. J., Park, S., & Agmon, N. (2009). Distance-dependent proton transfer along water wires connecting acid–base pairs. *The Journal of Physical Chemistry A*, *113*, 6599–6606.
60. Liu, W., Han, F., Smith, C., & Fang, C. (2012). Ultrafast conformational dynamics of pyranine during excited state proton transfer in aqueous solution revealed by femtosecond stimulated Raman spectroscopy. *The Journal of Physical Chemistry B*, *116*, 10535–10550.
61. Oscar, B. G., Liu, W., Rozanov, N. D., & Fang, C. (2016). Ultrafast intermolecular proton transfer to a proton scavenger in an organic solvent. *Physical Chemistry Chemical Physics*, *18*, 26151–26160.
62. Sheng, W., et al. (2018). Ultrafast dynamics of a “Super” photobase. *Angewandte Chemie International Edition*, *57*, 14742–14746.
63. Hunt, J. R., & Dawlaty, J. M. (2018). Photodriven deprotonation of alcohols by a quinoline photobase. *The Journal of Physical Chemistry A*, *122*, 7931–7940.
64. Sittig, M., Tom, J. C., Elter, J. K., Schacher, F. H., & Dietzek, B. (2021). Quinoline photobasicity: Investigation within water-soluble light-responsive copolymers. *Chemistry—A European Journal*, *27*, 1072–1079.
65. Vester, M., Grueter, A., Finkler, B., Becker, R., & Jung, G. (2016). Biexponential photon antibunching: Recombination kinetics within the Förster-cycle in DMSO. *Physical Chemistry Chemical Physics*, *18*, 10281–10288.
66. Vester, M., Staut, T., Enderlein, J., & Jung, G. (2015). Photon antibunching in a cyclic chemical reaction scheme. *The Journal of Physical Chemistry Letters*, *6*, 1149–1154.
67. Offenbacher, H., Wolfbeis, O. S., & Furlinger, E. (1986). Fluorescence optical sensors for continuous determination of near-neutral pH values. *Sensors and Actuators*, *9*, 73–84.
68. Clasen, A., et al. (2019). Kinetic and spectroscopic responses of pH-sensitive nanoparticles: Influence of the silica matrix. *RSC Advances*, *9*, 35695–35705.
69. Grandjean, A., Pérez Lustres, J. L., Muth, S., Maus, D., & Jung, G. (2021). Steady-state spectroscopy to single out the contact ion pair in excited-state proton transfer. *The Journal of Physical Chemistry Letters*, *12*, 1683–1689.
70. Grandjean, A., Pérez Lustres, J. L., & Jung, G. (2021). Solvent-controlled intermolecular proton-transfer follows an irreversible Eigen-Weller model from fs to ns. *ChemPhotoChem*, *5*, 1094–1105.
71. Megerle, U., Pugliesi, I., Schriever, C., Sailer, C. F., & Riedel, E. (2009). Sub-50 fs broadband absorption spectroscopy with tunable excitation: Putting the analysis of ultrafast molecular dynamics on solid ground. *Applied Physics B*, *96*, 215–231.
72. Schott, S., Steinbacher, A., Buback, J., Nuernberger, P., & Brixner, T. (2014). Generalized magic angle for time-resolved spectroscopy with laser pulses of arbitrary ellipticity. *Journal of Physics B: Atomic, Molecular and Optical Physics*, *47*, 124014.
73. Ruetzel, S., Kullmann, M., Buback, J., Nuernberger, P., & Brixner, T. (2013). Tracing the steps of photoinduced chemical reactions in organic molecules by coherent two-dimensional electronic spectroscopy using triggered exchange. *Physical Review Letters*, *110*, 148305.
74. Selig, U., et al. (2013). Similarities and differences in the optical response of perylene-based hetero-bichromophores and their monomeric units. *ChemPhysChem*, *14*, 1413–1422.
75. van Stokkum, I. H., Larsen, D. S., & van Grondelle, R. (2004). Global and target analysis of time-resolved spectra. *Biochimica et Biophysica Acta (BBA)-Bioenergetics*, *1657*, 82–104.
76. Marciniak, H., & Lochbrunner, S. (2014). On the interpretation of decay associated spectra in the presence of time dependent spectral shifts. *Chemical Physics Letters*, *609*, 184–188.
77. Consani, C., Berberich, M., Würthner, F., & Brixner, T. (2017). Ultrafast isomerization in a difluoroboryl-coordinated molecular switch. *Chemical Physics Letters*, *683*, 83–90.
78. Bolze, T., Wree, J.-L., Kanal, F., Schleier, D., & Nuernberger, P. (2018). Ultrafast dynamics of a fluorescent tetrazolium compound in solution. *ChemPhysChem*, *19*, 138–147.
79. Khah, A. M., Grimmelsmann, L., Knorr, J., Nuernberger, P., & Hättig, C. (2018). How a linear triazene photoisomerizes in a volume-conserving fashion. *Physical Chemistry Chemical Physics*, *20*, 28075–28087.
80. Brandl, F., Bergwinkl, S., Allacher, C., & Dick, B. (2020). Consecutive photoinduced electron transfer (conPET): The mechanism of the photocatalyst rhodamine 6G. *Chemistry—A European Journal*, *26*, 7946–7954.
81. Schott, S., Ress, L., Hrušák, J., Nuernberger, P., & Brixner, T. (2016). Identification of photofragmentation patterns in trihalide anions by global analysis of vibrational wavepacket dynamics in broadband transient absorption data. *Physical Chemistry Chemical Physics*, *18*, 33287–33302.
82. van Stokkum, I. H. M., et al. (2016). Estimation of damped oscillation associated spectra from ultrafast transient absorption spectra. *The Journal of Chemical Physics*, *145*, 174201.
83. Braver, Y., Gelzinis, A., Chmeliov, J., & Valkunas, L. (2019). Application of decay- and evolution-associated spectra for molecular systems with spectral shifts or inherent inhomogeneities. *Chemical Physics*, *525*, 110403.
84. Beckwith, J. S., Rumble, C. A., & Vauthey, E. (2020). Data analysis in transient electronic spectroscopy—an experimentalist’s view. *International Reviews in Physical Chemistry*, *39*, 135–216.
85. Horng, M. L., Gardecki, J. A., Papazyan, A., & Maroncelli, M. (1995). Subpicosecond measurements of polar solvation dynamics: Coumarin 153 revisited. *The Journal of Physical Chemistry*, *99*, 17311–17337.
86. Dobryakov, A. L., Pérez Lustres, J. L., Kovalenko, S. A., & Ernsting, N. P. (2008). Femtosecond transient absorption with chirped pump and supercontinuum probe: Perturbative calculation of

- transient spectra with general lineshape functions, and simplifications. *Chemical Physics*, 347, 127–138.
87. Kumpulainen, T., Lang, B., Rosspointner, A., & Vauthey, E. (2017). Ultrafast elementary photochemical processes of organic molecules in liquid solution. *Chemical Reviews*, 117, 10826–10939.
  88. Spry, D. B., Goun, A., Bell, C. B., & Fayer, M. D. (2006). Identification and properties of the  $^1L_a$  and  $^1L_b$  states of pyranine. *The Journal of Chemical Physics*, 125, 144514.
  89. Lessing, H. E., & Von Jena, A. (1976). Separation of rotational diffusion and level kinetics in transient absorption spectroscopy. *Chemical Physics Letters*, 42, 213–217.
  90. Fleming, G. R. (1986). *Chemical applications of ultrafast spectroscopy*. Oxford Univ. Press.
  91. Jonas, D. M., Lang, M. J., Nagasawa, Y., Joo, T., & Fleming, G. R. (1996). Pump–probe polarization anisotropy study of femtosecond energy transfer within the photosynthetic reaction center of rhodobacter sphaeroides R26. *The Journal of Physical Chemistry*, 100, 12660–12673.
  92. Arnett, D. C., Moser, C. C., Dutton, P. L., & Scherer, N. F. (1999). The first events in photosynthesis: Electronic coupling and energy transfer dynamics in the photosynthetic reaction center from rhodobacter sphaeroides. *The Journal of Physical Chemistry B*, 103, 2014–2032.
  93. Shaw, G. B., Brown, C. L., & Papanikolas, J. M. (2002). Investigation of interligand electron transfer in polypyridyl complexes of Os(II) using femtosecond polarization anisotropy methods: Examination of  $Os(bpy)_3^{2+}$  and  $Os(bpy)_2(mab)^{2+}$ . *The Journal of Physical Chemistry A*, 106, 1483–1495.
  94. Nuernberger, P., Vogt, G., Gerber, G., Improt, R., & Santoro, F. (2006). Femtosecond study on the isomerization dynamics of NK88. I. Ground-state dynamics after photoexcitation. *The Journal of Chemical Physics* 125, 044512.
  95. Theisen, M., et al. (2009). Femtosecond polarization resolved spectroscopy: A tool for determination of the three-dimensional orientation of electronic transition dipole moments and identification of configurational isomers. *The Journal of Chemical Physics*, 131, 124511.
  96. Nuernberger, P., et al. (2011). Strong ligand–protein interactions revealed by ultrafast infrared spectroscopy of CO in the heme pocket of the oxygen sensor FixL. *Journal of the American Chemical Society*, 133, 17110–17113.
  97. Kutta, R. J., Archipowa, N., & Scrutton, N. S. (2018). The sacrificial inactivation of the blue-light photosensor cryptochrome from *Drosophila melanogaster*. *Physical Chemistry Chemical Physics*, 20, 28767–28776.
  98. Gera, R., Meloni, S. L., & Anna, J. M. (2019). Unraveling confined dynamics of guests trapped in self-assembled  $Pd_6L_4$  nanocages by ultrafast mid-IR polarization-dependent spectroscopy. *The Journal of Physical Chemistry Letters*, 10, 413–418.
  99. Shizuka, H. (1985). Excited-state proton-transfer reactions and proton-induced quenching of aromatic compounds. *Accounts of Chemical Research*, 18, 141–147.
  100. Knochenmuss, R., Solntsev, K. M., & Tolbert, L. M. (2001). Molecular beam studies of the “Super” photoacid 5-cyano-2-naphthol in solvent clusters. *The Journal of Physical Chemistry A*, 105, 6393–6401.
  101. Cohen, B., Segal, J., & Huppert, D. (2002). Proton transfer from photoacid to solvent. *The Journal of Physical Chemistry A*, 106, 7462–7467.
  102. Clower, C., Solntsev, K. M., Kowalik, J., Tolbert, L. M., & Huppert, D. (2002). Photochemistry of “Super” photoacids. 3. Excited-state proton transfer from perfluoroalkylsulfonyl-substituted 2-Naphthols. *The Journal of Physical Chemistry A*, 106, 3114–3122.
  103. Deshpande, A. V., Beidoun, A., Penzkofer, A., & Wagenblast, G. (1990). Absorption and emission spectroscopic investigation of cyanovinyl-diethylaniline dye vapors. *Chemical Physics*, 142, 123–131.
  104. Riedle, E., & Wenninger, M. Time resolved spectroscopy in photocatalysis. in *Chemical Photocatalysis* (ed. König, B.) (De Gruyter, 2013). doi:<https://doi.org/10.1515/9783110269246>.
  105. Maus, D., Grandjean, A., & Jung, G. (2018). Toward magic photoacids: Proton transfer in concentrated sulfuric acid. *The Journal of Physical Chemistry A*, 122, 9025–9030.